I&EC research
Industrial & Engineering Chemistry Research

Article

Cite This: *Ind. Eng. Chem. Res.* XXXX, XXX, XXX−XXX

pubs.acs.org/IECR

Computational Fluid Dynamics-Based Study of a High Emissivity Coil Coating in an Industrial Steam Cracker

Stijn Vangaever,[†] Pieter A. Reyniers,[†] Cor Visser,[‡] Dietlinde Jakobi,[‡] Geraldine J. Heynderickx,[†] Guy B. Marin,[†] and Kevin M. Van Geem*,[†]

[†]Ghent University, Laboratory for Chemical Technology, Technologiepark 914, 9052 Ghent, Belgium

[‡]Schmidt + Clemens GmbH + Co. KG, Kaiserau 2, 51789 Lindlar, Germany

Supporting Information

ABSTRACT: To assess the effect of applying a high emissivity coating to the reactor coils in a steam cracking furnace, a complete energy balance was made for two cases based on simulations of the radiant section, reactors, convection section, and transfer line exchanger. A base case with a typical emissivity spectrum for a generic high-alloy steel was compared to a case with an artificially increased emissivity corresponding to a high emissivity coating. At the same cracking severity, coating the radiant coils increases the radiant section efficiency by 0.70% absolute, reduces the required furnace firing rate by 1.73%, and reduces the flue gas bridge wall temperature by 14 K. Minor changes to the convection section layout are required to compensate for the shift in duty to the radiant section: the reactor feed is still fully preheated to the targeted crossover temperature, but the production of high pressure steam is reduced.

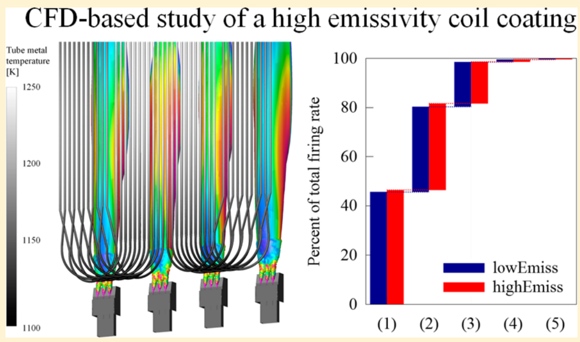

1. INTRODUCTION

In many high temperature applications, radiation is the dominant heat transfer mechanism. Heat transfer via radiation between two surfaces mainly depends on the view factor between the two surfaces and the temperatures of both surfaces. However, the radiative properties of the surfaces, in particular their emissivity, also determine the total amount of heat transferred between the surfaces. Therefore, for dedicated applications, coatings modifying the surface radiative properties are used when two radiative sources are at different temperatures. These spectrally selective coatings allow tuning of the radiative properties in specific wavelength bands, depending on whether reflection or absorption is desired.[1] A well-known example improves the efficiency of solar-thermal conversion via a coating that increases the absorptivity of the highly energetic solar radiance and reduces the emittance in the lower infrared region.[2] In contrast, radiative cooling by reducing the absorptivity of electromagnetic radiation in the visible spectrum and increasing the emittance in the lower infrared spectrum increases the lifetime of materials used in aerospace applications.[3] Analogously, the electrical resistance of above-ground power lines is decreased by lowering their temperature via radiative cooling. The spectrally selective surface coating prevents the conductor from absorbing solar radiation and emits radiation at wavelengths with high intensities at typical power line operating temperatures. Preventing a temperature rise due to solar radiation allows for keeping the electrical conductivity of the power line as high as possible and hence minimizing the losses. Passive radiative cooling to a surface temperature below ambient air temperature by multilayered coatings could have a significant impact on global energy consumption. In the work of Raman et al., the total power radiated by a modified surface exceeds the sum of the absorbed solar irradiance, the thermal radiation, and the conductive and convective heat transfer contributions.[4] Due to this net negative energy balance, a surface can be cooled to a temperature below the ambient air temperature under direct sunlight.

The emissivity of a surface is determined by a number of factors, including but not limited to wavelength, surface roughness, surface chemical composition, surface impurities, and surface temperature.[5] A particular strategy in high-temperature applications to change the radiative properties of a surface is applying high emissivity coatings. Whereas solid surfaces typically absorb and emit radiation at all frequencies, gases absorb and emit radiation at certain discrete wavelengths only, which depend on the rotational and vibrational energy levels of the optically active molecules in the gas. High emissivity coatings in fired heaters aim at minimizing the amount of radiation absorbed by the flue gas while maximizing the amount of radiation emitted by the surface over the full wavelength spectrum. This is done by sending proportionally more radiation through the wavelength bands in the gas phase

Received: August 23, 2018
Revised: November 9, 2018
Accepted: November 14, 2018
Published: November 14, 2018

DOI: 10.1021/acs.iecr.8b04068
Ind. Eng. Chem. Res. XXXX, XXX, XXX−XXX

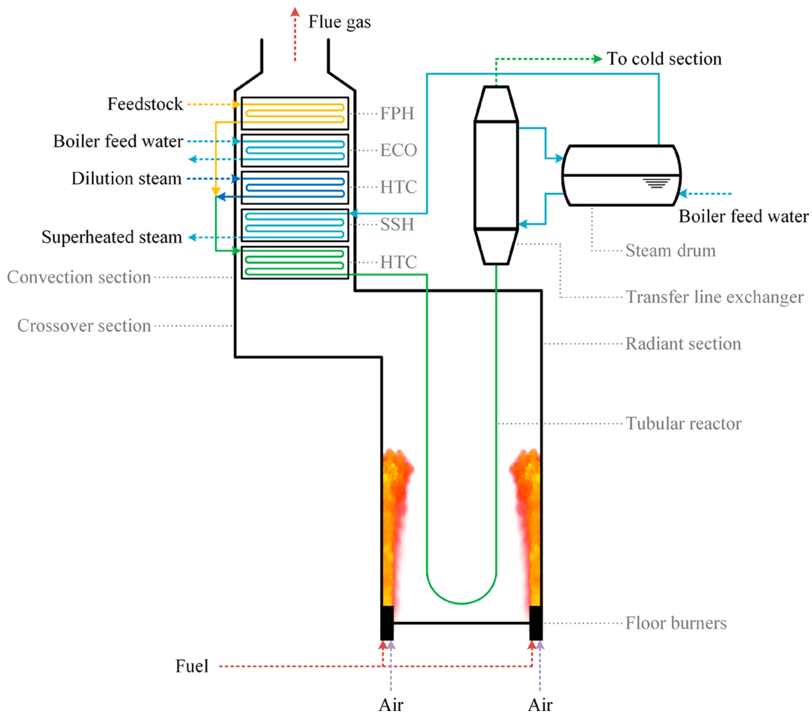

Figure 1. Schematic drawing of a steam cracking unit.

that are transparent for infrared radiation, i.e., the wavelength bands for which the molecules in the flue gas are optically inactive. In the glass industry and the iron and steel industry, high emissivity coatings are already applied on the refractory walls of fired heaters in order to improve radiative heat transfer and hence reduce energy consumption.[6,7]

This work aims to assess the effect of applying high emissivity coatings to the radiant coils of a steam cracking unit on the energy balance of an entire steam cracking unit under start-of-run conditions. Steam cracking is the leading technology to produce light olefins, including ethene and propene, starting from a wide range of hydrocarbon feedstocks. A steam cracker consists of a number of sections that are closely coupled in terms of energy and mass balances: the radiant section or furnace including the tubular reactors, the convection section, the transfer line exchanger (TLE), and the steam drum, all of which are represented on Figure 1. A hydrocarbon feedstock is evaporated, mixed with dilution steam, and further preheated in the convection section. Part of the residual thermal energy in the flue gas of the radiant section is used for this feed preheat. The remainder is used to evaporate boiler feedwater and to superheat high pressure steam. The preheated mixture of hydrocarbons and steam passes through one of multiple tubular reactors suspended in the radiant section, where floor and/or wall burners provide the necessary heat for the chemical reactions. The reactor effluent passes through the TLE, where it is cooled down as fast as possible to stop the reactions. The quenched cracked gas then goes to the cold section for separation. The heat from cooling the reactor effluent in the TLE is used to evaporate boiler feedwater (BFW) at high pressure. The generated saturated steam is further superheated in the aforementioned heat exchanger in the convection section.

Over the past decade, significant progress has been made in modeling the radiant section of steam cracking units.[8−10] Initially, computational fluid dynamics (CFD) to account for flow dynamics and Hottel's zone method to model the radiative heat transfer were combined.[11] With the increase in computational power over the years, radiative heat transfer can be calculated on the CFD grid as well.[8,9] Habibi et al. investigated the impact of radiation models in CFD simulations of steam cracking furnaces.[12] Stefanidis et al. determined that nongray gas models are required to accurately model the radiative heat transfer in steam cracking furnaces since gray gas models tend to overpredict the furnace thermal efficiency by 5%.[13] This corresponds to the "gray gas myth," as stated by Edwards and Balakrishnan, claiming that treating the flue gas as a gray gas in combustion applications can lead to temperature underpredictions of 100 K and more.[14,15] Recently, in the work of Zhang et al., coupled CFD-based furnace-reactor simulations of an industrial steam cracker were performed, evaluating the impact of flue gas radiative properties, burner geometry, and feedstock distribution over the reactor coils.[16−18] The computational framework based on coupled furnace-reactor simulations was even used for run length predictions.[19] Several authors also investigated the effects of high emissivity coatings on the energy balance of a furnace. Heynderickx and Nozawa[20,21] used the furnace model based on Hottel's zone method to investigate the effect of coating both the furnace wall and the reactor tubes, with particular attention for how the gas-phase and surface radiative properties were implemented. The coating increased the weighted average of the spectral emissivity values by 180% for the refractory and by 60% for the tube outer walls.

In case of applying the coating only to the reactors, the simulated furnace efficiency increased from 39.14% to 42.66%. When applying the same coating to both the refractory and the reactor tubes, the simulated furnace efficiency even increased to 44.26%. Stefanidis et al.[22] used a computational fluid dynamics simulation of the radiant section to assess the effect of a coating on the energy balance and the reactor performance of a naphtha steam cracking unit. Increasing the weighted

DOI: 10.1021/acs.iecr.8b04068
Ind. Eng. Chem. Res. XXXX, XXX, XXX−XXX

Table 1. Simplified Combustion Mechanism and Associated Reaction Rate Expressions[16]

reaction	reaction rate [mol/m^3/s]
$CH_4 + 1.5O_2 \rightarrow CO + 2H_2O$	$r_{CH_4} = 1.5 \times 10^7 \exp\left(-\frac{125580}{RT}\right)C_{CH_4}^{-0.3}C_{O_2}^{1.3}$
$C_2H_4 + 2O_2 \rightarrow 2CO + 2H_2O$	$r_{C_2H_4} = 7.589 \times 10^7 \exp\left(-\frac{125580}{RT}\right)C_{C_2H_4}^{-0.1}C_{O_2}^{1.65}$
$CO + 0.5O_2 \rightarrow CO_2$	$r_{CO} = 1.259 \times 10^{10} \exp\left(-\frac{167430}{RT}\right)C_{CO}C_{O_2}^{0.25}C_{H_2O}^{0.5}$
$H_2 + 0.5O_2 \rightarrow H_2O$	$r_{H_2} = 10^4 C_{H_2}C_{O_2}^{0.25}$

spectral emissivity of the refractory by 180% via a coating increased the simulated furnace efficiency from 40.0% to 40.9%. Although the radiative properties of the considered furnace and coating were the same for Heynderickx and Nozawa and Stefanidis et al., the simulated increase in furnace efficiency of Stefanidis et al. is less than that of Heynderickx and Nozawa. Stefanidis et al. used a CFD-based approach to model the furnace while Heynderickx and Nozawa relied on a Monte Carlo-based simulation framework with a coarse computational grid. The inconsistency in the simulated increase in furnace efficiency results in some uncertainty on the effect of the coating. Additionally, neither considered the effect of the changed efficiency of the radiant section on the other units of the hot section of a steam cracker, in particular the transfer line exchanger and the convection section.

In the present work, two furnace-reactor simulations are performed, one with an industrially relevant reactor coil emissivity and one with a higher reactor coil emissivity, corresponding to that of radiant coils coated with a high emissivity coating. To assess the impact of coated radiant coils on the complete energy balance of a steam cracking unit, not only the radiant section is modeled using coupled furnace–reactor simulations but also the transfer line exchanger and the convection section. The goal is to assess the potential operational benefits of applying a high emissivity coating to the reactor outer wall in a steam cracking furnace.

2. MATHEMATICAL MODELS

The governing equations and closure models are only briefly described. For a more detailed discussion on the furnace–reactor simulations, the reader is referred to Zhang et al.[16] For further details on the convection section simulations, the reader is referred to Verhees et al.[23]

2.1. Tubular Reactors. Given the nonisothermal, non-adiabatic, and nonisobaric nature of the steam cracking process, the one-dimensional conservation equations for the species, momentum, and energy have to be solved. The corresponding set of ordinary differential equations reads:

$$\frac{dF_j}{dz} = \frac{\pi d^2}{4}R_j \tag{1}$$

$$-\frac{dp}{dz} = \left(\frac{2f}{d} + \frac{\zeta}{\pi r_b}\right)\rho u^2 + \rho u\frac{du}{dz} \tag{2}$$

$$\sum_{j=1}^{n_{spec}} F_j c_{p,j}\frac{dT}{dz} = \pi d q + \frac{\pi d^2}{4}\sum_{i=1}^{N_R} r_i(-\Delta H_i) \tag{3}$$

These one-dimensional reactor model equations are solved using the commercial software package COILSIM1D 3.8.[24] Integration of this set of nonlinear first order differential equations results in profiles for product yields, pressure, and temperature as a function of the axial coordinate along the centerline. The local heat flux to the reactors, q, is obtained from 3D furnace simulations described in section 2.2.

2.2. Radiant Section. *2.2.1. Governing Equations and Turbulence Model.* The three-dimensional steady-state global mass, momentum, energy, and species conservation equations for a compressible, reacting fluid have to be solved.

$$\nabla\cdot(\rho\overline{u}) = 0 \tag{4}$$

$$\nabla\cdot(\rho\overline{u}\overline{u}) = -\nabla p + \nabla\cdot(\overline{\overline{\tau}}) + S_M \tag{5}$$

$$\nabla\cdot(\overline{u}(\rho E + p)) = \nabla\cdot\left(k_{eff}\nabla T - \sum_{j=1}^{n_{spec}} h_j\overline{J}_j + (\overline{\overline{\tau}}\cdot\overline{u})\right) + S_h \tag{6}$$

$$\nabla\cdot\left(\frac{\overline{u}Y_j}{V_m}\right) = -\nabla\cdot\overline{J}_j + R_j \tag{7}$$

where gravity is the only source term in the momentum equation, S_M, and the energy source term, S_h, is the net volumetric heat duty due to radiation and reactions. For reasons of computational cost, the conservation equations are Favre-averaged to the Reynolds-averaged Navier–Stokes (RANS) equations. The Boussinesq hypothesis relates the resulting Reynolds stresses to the mean velocity gradients in order to close the unclosed terms.[25] The renormalization group (RNG) k-ε model is employed to calculate the turbulent viscosity as it provides acceptable results for the particular application. The governing equations are solved using the commercial software package ANSYS Fluent 15.0.7.

The temperature of the outer wall of the reactors is obtained from COILSIM1D. The heat flux through the wall is calculated according to eq 8. Section 2.2.3 provides more details on the calculation of the radiation term q_{rad}. Convective heat transfer to the wall is proportional to the difference in temperature between the wall and the adjacent fluid cell with the convective heat transfer coefficient h_f as the proportionality coefficient, calculated using the analogy between heat and momentum transfer.[26] The enhanced wall treatment option of ANSYS Fluent is used, separating the boundary layer in a viscosity-affected region and a fully turbulent region and providing appropriate blending function to ensure a smooth transition between the two layers.

$$q = h_f(T_w - T_f) + q_{rad} \tag{8}$$

2.2.2. Combustion Model. A simplified two-step combustion model proposed by Westbrook and Dryer[27] is used to

DOI: 10.1021/acs.iecr.8b04068
Ind. Eng. Chem. Res. XXXX, XXX, XXX−XXX

obtain the reaction rates for the fuel combustion. The reactions and the associated kinetic parameters are taken from the work of Stefanidis et al.[28] and Zhang et al.[16] and are given in Table 1. The turbulence–chemistry interaction is accounted for via the finite-rate/eddy-dissipation model.[29,30] By assuming that the chemical reactions are fast compared to mixing, the rate of reaction can be related to the eddy mixing time scale, i.e., the rate of mixing on the smallest turbulent scales. The original eddy dissipation model was extended to consider the case when the combustion reactions are slower than mixing, for example, in zones with a low temperature. The Arrhenius reaction rate is added as a switch to indicate the kinetically governed flame region. The net reaction rate is calculated as the minimum of the Arrhenius reaction rate and the eddy dissipation reaction rate.

2.2.3. Radiation Model. The discrete ordinates (DO) radiation model is the preferred model to solve the radiative transfer equation in full-scale industrial furnace simulations.[12,18] The nongray implementation of the DO model is used to solve the radiative transfer equation for the spectral intensity I_i in a selected number of wavelength bands for a finite number of discrete solid angles. Due to the low tendency for the fuel to form soot, scattering of radiation can be neglected, resulting in the following radiative transfer equation for the ith band at position $\vec{r}$ in direction $\vec{s}$.[31]

$$\nabla\cdot(I_i(\vec{r}, \vec{s})\vec{s}) + \kappa_i I_i(\vec{r}, \vec{s}) = \kappa_i I_{\mathrm{b},i} \tag{9}$$

where κ_i is the absorption coefficient and $I_{\mathrm{b},i}$ is the blackbody intensity for the ith band given by the Planck law.

$$I_{\mathrm{b},i} = [f(n\lambda_{\mathrm{u},i}T) - f(n\lambda_{\mathrm{l},i}T)]\frac{T^4}{n\pi(\lambda_{\mathrm{u},i} - \lambda_{\mathrm{l},i})} \tag{10}$$

where $\lambda_{\mathrm{u},i}$ and $\lambda_{\mathrm{l},i}$ are the upper and the lower wavelength limits of the ith wavelength band, respectively, and n is the refractive index. The fraction of radiant energy, $f(n\lambda T)$, emitted in the wavelength interval from 0 to λ can be described by the infinite series

$$f(n\lambda T) = \frac{15}{\pi^4}\sum_{m=1}^{\infty}\frac{\mathrm{e}^{-m\zeta}}{m^4}[6 + 6(m\zeta) + 3(m\zeta)^2 + (m\zeta)^3], \zeta = \frac{hc}{nk_{\mathrm{B}}\lambda T} \tag{11}$$

where h is the Planck constant, c is the speed of light in a vacuum, and k_{B} is the Boltzmann constant. The spectral absorption coefficient of the gas in the ith band κ_i is obtained from the exponential wide band model (EWBM) proposed by Edwards and Balakrishnan[15] and later adopted by Stefanidis et al.[22] Zhang et al.[16] determined that five nontransparent absorption bands suffice to model the gas-phase absorptivity under steam cracking operating conditions. The absorption bands originate from rotational and translational modes of the optically active molecules carbon dioxide and water. Since one of the absorption bands of carbon dioxide overlaps with one of the absorption bands of water, these two bands are combined, resulting in four nontransparent windows in the infrared wavelength spectrum. Table 2 provides an overview of the four nontransparent windows and the five transparent windows for the flue gas of a steam cracking furnace. This nine-band EWBM is a compromise between the computationally more expensive narrow band models on the one hand and gray gas models on the other hand.

Table 2. Division of the Wavelength Spectrum Based on the Nine Band EWBM

				radiant coil emissivity [-]	
band	lower limit [μm]	upper limit [μm]	absorption coefficient [m^{-1}]	low emissivity	high emissivity
1	0.00	2.54	0	0.8472	0.9472
2	2.54	2.75	EWBM	0.8314	0.9314
3	2.75	4.15	0	0.8223	0.9223
4	4.15	4.47	EWBM	0.8120	0.9120
5	4.47	5.31	0	0.8046	0.9046
6	5.31	7.60	EWBM	0.7903	0.8903
7	7.60	12.55	0	0.7517	0.8517
8	12.55	18.68	EWBM	0.6870	0.7870
9	18.68	150.00	0	0.6389	0.7389

When solving the radiative transfer equation, reactor coils are treated as diffuse and opaque. In what follows, the absorptivity is set to be equal to the emissivity of a surface, according to the Kirchhoff law of thermal radiation. The incident radiative heat flux on a boundary surface in the ith wavelength band $q_{\mathrm{in},i}$ corresponds to

$$q_{\mathrm{in},i} = (\lambda_{\mathrm{u},i} - \lambda_{\mathrm{l},i})\int_{\vec{s}.\vec{n}>0} I_{\mathrm{in},i}\vec{s}.\vec{n}\ \mathrm{d}\Omega \tag{12}$$

The net radiative flux leaving the boundary surface in the ith wavelength is given by

$$q_{\mathrm{out},i} = (1 - \varepsilon_{\mathrm{w},i})q_{\mathrm{in},i} + \varepsilon_{\mathrm{w},i}[f(n\lambda_{\mathrm{u},i}T) - f(n\lambda_{\mathrm{l},i}T)]n^2\sigma T^4 \tag{13}$$

where the wall emissivity, $\varepsilon_{\mathrm{w},i}$, within the wavelength band defined by $\lambda_{\mathrm{u},i}$ and $\lambda_{\mathrm{l},i}$, is introduced. The nongray behavior of the boundary surfaces in general, and the reactor coils in particular, can be considered via the band-dependent surface emissivity $\varepsilon_{\mathrm{w},i}$.[22]

2.3. Transfer Line Exchanger. The quenching of the reactor effluent in the transfer line exchanger is calculated via the commercial software package COILSIM1D 3.8. Free thermosiphon operation is assumed for the TLE, implying that the mass flow on the water/steam sides is determined by buoyancy and natural convection. The same one-dimensional steady-state conservation equations for species, momentum, and energy as previously described in section 2.1 are used to simulate the process side of the TLE, implying that additional reaction is considered. The boundary condition on the water/steam side is set to a fixed temperature, corresponding to the saturation temperature of water at the considered pressure.

2.4. Convection Section. A dedicated 1D model CONVEC-1D developed by Verhees et al.[23] is used to determine the heat and mass balances over the convection section. The tool allows the specification of a number of interconnected banks with different functions to recover the remaining heat from the flue gas. For a detailed description of the implemented models, the reader is referred to the work of Verhees et al.;[23] only a summary will be given here.

On the process gas side, two situations occur: in the majority of the tubes, single-phase forced convection takes place, for which the Nusselt number can be calculated based on the Dittus–Boelter, Sieder–Tate, or Gnielinsky correlations. In the case of a liquid feed, two-phase flow boiling also takes place in a number of banks. Flow pattern maps, giving the flow regime (slug, intermittent, annular, mist, dry-out, stratified-

DOI: 10.1021/acs.iecr.8b04068
Ind. Eng. Chem. Res. XXXX, XXX, XXX−XXX

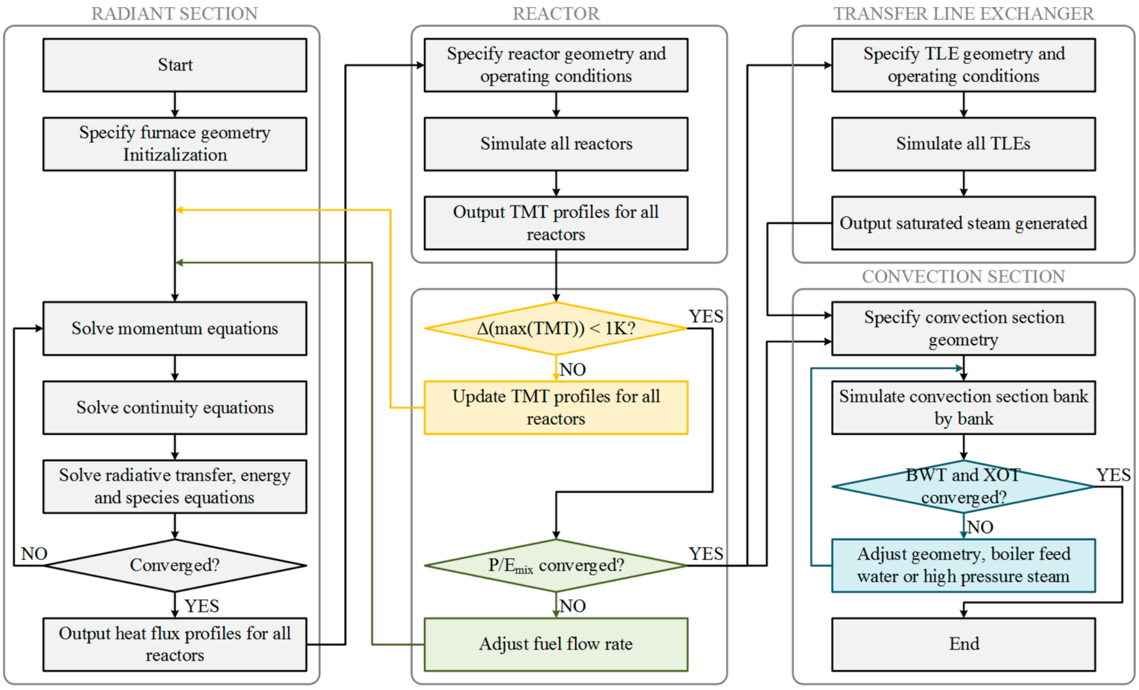

Figure 2. Solution strategy for coupled simulation of the radiant section, the reactors, the transfer line exchanger, and the convection section.

wavy, wavy, and stratified flow) as a function of the vapor quality and the mass flux, are required to determine the heat transfer rate. On the flue gas side, the analytical model developed by Khan et al.[32] is used to describe natural convection through a tube bundle.

$$Nu_D = C_1 Re_D^{1/2} Pr^{1/3} \tag{14}$$

where the coefficient C_1 takes the arrangement of the tube bank into account defined by the longitudinal, σ_L, and transverse pitch, σ_T, of the tube bank:

$$C_1 = \begin{cases} [0.25 + \exp(-0.55\sigma_L)] \sigma_L^{0.212} \sigma_T^{0.285} & \text{for inline arrangement} \\ \dfrac{0.61\sigma_L^{0.091}\sigma_T^{0.053}}{1 - 2\exp(-1.09\sigma_L)} & \text{for staggered arrangement} \end{cases} \tag{15}$$

For a circular finned geometry, the fin efficiency using the relations described by Shah was used.[33] Discrete ordinate CFD calculations using the previously described EWBM approach were used to define an empirical correlation between radiative heat flux and local flue gas temperature. This correlation was consequently used in the 1D simulations of the convection section to reduce computational time. The obtained correlation is geometry dependent so for a different convection section geometry, an analogous hybrid 3D−1D modeling approach is suggested.[34]

The convection section model is solved tube row by tube row from top to bottom, in the logical sequence for the process fluid. This implies that the stack temperature, the temperature of the flue gas leaving the convection section through the stack, is to be estimated in the first iteration of the solution. In subsequent iterations, the estimate is updated in order to match the bridge wall temperature (BWT), the inlet temperature of the flue gas in the convection section, to the results from the radiant section simulation. During the simulation, the convection section is considered tube row by tube row from top to bottom, resulting in heat flux profiles and temperature profiles along the axial coordinate for a generic tube at that height in the convection section on the one hand and the resulting flue gas mixing cup temperature on the other hand. As the tool is one-dimensional, the profiles for the process gas side only depend on the axial coordinate in the tube at that height in the furnace while for the flue gas side, the profile only depends on the height in the furnace. This however is sufficient to determine the full heat and mass balance over the convection section.

2.5. Steam Drum. As the main function of the steam drum is phase separation of saturated steam and saturated boiler feedwater, it is sufficient to solve the steady-state conservation equation only for mass and energy. The vessel is assumed to operate adiabatically. It introduces a two-fold coupling between the transfer line exchanger and the convection section: on the one hand, the amount of boiler feedwater preheated in the economizer of the convection section is equal to the amount of saturated steam generated in the TLE, and on the other hand, the amount of saturated steam generated in the TLE is equal to the amount of steam superheated in the high pressure steam superheater banks of the convection section. These couplings are considered implicitly in the solution strategy, see section 2.6, so the mass and energy balances over the steam drum are not explicitly calculated.

2.6. Solution Strategy. Figure 2 illustrates the solution strategy for the coupled units in a steam cracker. The four units described in the previous paragraphs, i.e., radiant section, tubular reactors, transfer line exchanger, and convection section, are shown, including the feedback loops within each unit and between units. The simulation strategy starts by specifying the geometry and the operating conditions for the radiant section, completed with initial estimates for the tube metal temperature (TMT) profiles of the reactor coils suspended in the radiant section. The computational fluid dynamics simulation is run to convergence, and the net heat

DOI: 10.1021/acs.iecr.8b04068
Ind. Eng. Chem. Res. XXXX, XXX, XXX−XXX

flux to each of the reactor coils as a function of the reactor coil axial coordinate is extracted to be used as a boundary condition for the reactor simulation. Indeed, based on the heat flux profile from the radiant section, the reactor simulations provide axial profiles for all relevant process variables, in particular TMT profiles. This update for the TMT profiles is specified as the new boundary condition in the radiant section simulation. This feedback loop, indicated in gold in Figure 2, continues until for each coil the difference between the maximum TMT predicted in two subsequent simulations is smaller than 1 K.

Once the coupled furnace−reactor simulation has been completed, the TLE is calculated to obtain the final product composition after quenching and to obtain the amount of steam generated. The amount of saturated steam generated is important since it determines the flow rates of the process fluid through the energy recovery banks in the convection section.

The convection section is calculated last. As the coil inlet temperature is fixed in the reactor simulations, the coupling between the convection section and the radiant section is not considered via an iterative procedure as was done for the coupling between the radiant section and the reactors. Instead, the process conditions in the convection section are set such that it provides results that are consistent with what was previously calculated for the reactors and the TLE. In other words, on the flue gas side, the stack gas temperature is adjusted iteratively until the BWT matches the outlet temperature of the flue gas in the furnace calculations. On the process gas side, the crossover temperature (XOT) is forced to match the coil inlet temperature of the reactor simulations. Any heat loss from the process gas that might occur between the convection section and the furnace is disregarded. For the reference low emissivity case, this implies that the following quantities are fixed for reasons of consistency: boiler feedwater outlet temperature (ECO), hydrocarbon feed outlet temperature (HTC-III), boiler feedwater flow rate (ECO), and high pressure steam flow rate (HPSSH-I). For the high emissivity case, the boiler feedwater flow rate and the size of the fins on the convection section tubes can be adjusted in order to sufficiently preheat the hydrocarbon feed, while keeping the same cracking severity.

3. CASE-SPECIFIC GEOMETRIC AND OPERATING CONDITIONS

Two cases are considered in this work that differ in the radiative properties of the reactor coils to investigate the effect of a high emissivity coating on the heat and mass balance of a complete steam cracking unit. In what follows, the base case with uncoated reactors is referred to as the low emissivity case while the case with the coated reactors is referred to as the high emissivity case.

3.1. Radiant Section and Reactors. The geometric details and operating conditions for the naphtha steam cracking unit are identical to those previously modeled by Zhang et al.[16] Only one-fourth of the ultra selective conversion (USC) furnace is simulated to reduce the computational cost. Figure 3 illustrates the furnace geometry: two sets of 11 U-coil reactors are suspended in middle of the simulated part of the furnace. At either side of the tubes, four floor burners are equidistantly positioned next to the refractory wall. A detailed overview of the geometry and operating conditions is given in the Supporting Information Table S1. In the low emissivity case, the emissivity of the reactor coils in each band is set to that of a generic high-alloy steel. In the high emissivity case, the emissivity of the reactor coils is set to that of a coated metal. The emissivity values of the reactor coils in the nine bands considered by the EWBM model for both cases are given in Table 2. The emissivity of the refractory wall is set to a constant value of 0.75.

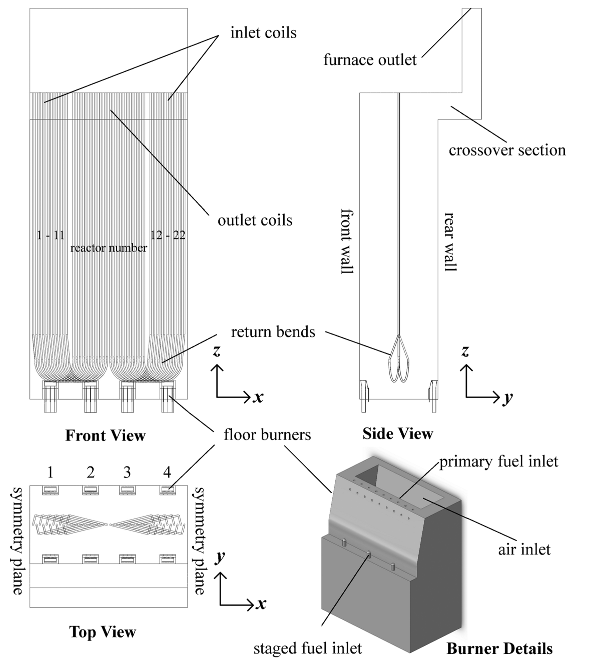

Figure 3. Schematic representation of the simulated segment of the Ultra Selective Conversion furnace[16,19] (Adapted with permission from Zhang et al.[16] Copyright 2015 John Wiley and Sons).

To allow a fair comparison between the reference case with the low tube wall emissivity and the improved case with the higher tube wall emissivity, the cracking severity is fixed.

The propene-to-ethene mass ratio at the outlet of coil i, $(P/E)_i$, is used as the cracking severity index.[35] The averaged cracking severity over n_r coils, referred to as the mixing-cup averaged propene-to-ethene mass ratio $(P/E)_{mix}$ is the mixing-cup average of the propene to ethene mass ratios of each individual coil:

$$(P/E)_{mix} = \frac{\sum_{i=1}^{n_r} (P/E)_i \dot{m}_i}{\sum_{i=1}^{n_r} \dot{m}_i} \tag{16}$$

The fuel flow rate in the high emissivity case is adjusted in order to match the mixing-cup averaged P/E ratio obtained from the reference case with the low tube wall emissivity. Due to the nonlinearity of the problem, adjusting the fuel flow rate in the high emissivity case is done iteratively, indicated by the green feedback loop in Figure 2. Convergence is achieved when the relative difference between the $(P/E)_{mix}$ values of the high emissivity case and the low emissivity case is smaller than 0.01%. The total fuel flow rate to the eight burners for the low emissivity case is 0.2777 kg/s.

3.2. Transfer Line Exchanger. The process gas effluent from two adjacent reactor coils is mixed in an adiabatic manifold and subsequently cooled rapidly in the transfer line exchanger. The geometry is based on the ultraselective exchanger quench cooler, a straight jacketed tube with process gas flowing in the inner tube and boiler feedwater flowing

DOI: 10.1021/acs.iecr.8b04068
Ind. Eng. Chem. Res. XXXX, XXX, XXX−XXX

inside the jacket.[36] The length of the TLE is adjusted to obtain process gas outlet temperatures between 770 and 780 K. At this temperature, all cracking reactions are stopped so further changes in the effluent composition are avoided. However, the process gas is to be cooled further before it can be further processed in the separation section, so the primary TLE is followed by a secondary shell-and-tube type TLE that further cools the process gas. Typical temperatures for the cracked gas leaving the secondary TLE depend on the feedstock type, varying from 570 K for a gaseous feedstock to 690 K for naphtha feedstocks, to even higher temperatures for atmospheric gas oils.[36] Higher temperatures are required for heavier feeds to avoid excessive fouling due to condensation coke formation. In this work, only the primary TLE is simulated, as the secondary TLE will be identical in the low emissivity case and high emissivity case and hence has no influence on the conclusions. The geometric details and operating conditions of the adiabatic section and the TLE are summarized in the Supporting Information, Table S2. The simulation provides information about the axial profiles for the process gas in the TLE tubes and the amount of steam generated.

3.3. Convection Section. The number of tube banks in the convection section is identical to that in the convection section simulated by Verhees et al.[23] The order of the eight banks, their interconnection, and the input and output streams are shown in Figure 4. Details on the tube configuration and layout of each tube bank are summarized in Table S3 in the Supporting Information. The properties of the feed streams labeled "S" can be found in Table 3.

The hydrocarbon feedstock (S1) is fed to the feed preheater (FPH) and subsequently mixed with part of the dilution steam (S3) to ensure full evaporation. The hydrocarbon−steam mixture then passes through the first and second high temperature convection banks (HTC-I and HTC-II). The outflow of HTC-II is mixed with the outflow of the dilution steam superheater (DSSH) before being sent to the third high temperature convection bank (HTC-III) where the process gas is heated to the crossover temperature. In this work, the coil inlet temperature is assumed to be equal to the crossover temperature, i.e., any heat loss that the process gas might suffer between the convection section and the furnace is disregarded. The economizer bank (ECO) is used to preheat boiler feedwater to 10 K below the saturation temperature at the considered pressure. It is assumed that this water is completely evaporated in the transfer line exchangers to close the mass and energy balance over the steam drum. Saturated high pressure steam generated by the TLE is superheated in the high pressure steam superheaters (HPSSH-I and HPSSH-II).

For the high emissivity case, additional criteria are imposed on the simulation to allow fair comparison with the low emissivity case. In particular, the following quantities are fixed to the value obtained from the low emissivity case: flue gas stack temperature and high pressure steam outlet temperature (HPSSH-II). The flow rate of inlet stream S6, see Table 3, and the layout of the fins on the steam superheating bank HPSSH-II are adjusted to shift power between banks.

4. RESULTS AND DISCUSSION

4.1. Radiant Section and Reactor. An overview of the most important results of the coupled furnace−reactor simulations for both the low emissivity and high emissivity cases is found in Table 4. Although only one-fourth of the radiant section and the reactors was simulated explicitly, Table 4 reports the values for the complete radiant section. The results related to the reactors are very similar in both cases, as was the intention since the cracking severity expressed via the mixing-cup averaged P/E is the same. Total absorbed heat and average yields of propene and ethene are nearly identical in the low emissivity and the high emissivity cases, pointing to equal reactor performance in each case. Small differences can be related to the thresholds set as convergence criteria for the

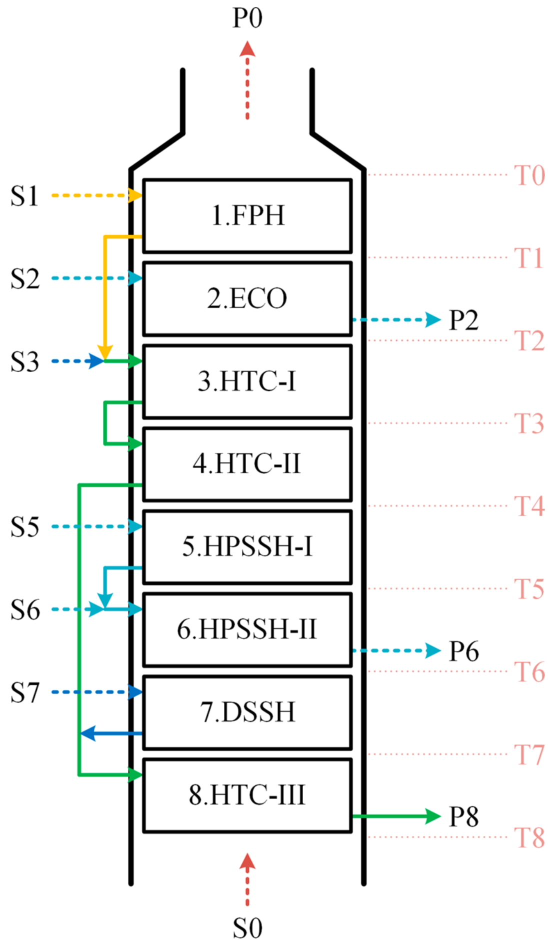

Figure 4. Schematic representation of the simulated convection section. Arrows labeled "S" represent feed streams. Arrows labeled "P" represent product streams. The labels "T" represent flue gas temperature measurement points.

Table 3. Operating Conditions of the Convection Section: Inlet Streams

stream	name	temperature [K]	pressure [bar]	mass flow rate [kg/s] low emissivity	mass flow rate [kg/s] high emissivity
S1	hydrocarbon feed	333	6.1	8.044	
S2	boiler feedwater	418	121.0	6.211	6.197
S3	dilution steam 1	458	5.8	0.670	
S5	high pressure steam 1	597	118.7	6.211	6.197
S6	high pressure steam 2	418	117.9	0.229	0.000
S7	dilution steam 2	458	5.2	3.352	

DOI: 10.1021/acs.iecr.8b04068
Ind. Eng. Chem. Res. XXXX, XXX, XXX−XXX

Table 4. Results of the Coupled Furnace-Reactor Simulations for Both the Low Emissivity Case and the High Emissivity Case

	low emissivity	high emissivity
radiant section		
total fuel flow rate [kg/s]	1.1108	1.0916
total air flow rate [kg/s]	21.184	20.816
air to fuel ratio [-]	19.07	19.07
flue gas mass flow rate [kg/s]	22.296	21.908
flue gas bridge wall temperature [K]	1370	1356
average maximum TMT [K]	1235.36	1235.21
total radiative heat flux to all reactors [kW]	20144	20484
percent of total heat flux via radiation [%]	77.88	79.33
reactor		
mixing-cup average COT [K]	1146.1	1145.3
average propene yield [wt %]	15.25	15.25
average ethene yield [wt %]	28.89	28.88
mixing-cup average *P/E*	0.5284	0.5284
total heat flux to all reactors [kW]	25868	25820
transfer line exchanger		
total water flow rate [kg/s]	67.514	67.300
total steam produced [kg/s]	6.440	6.426
total exchanged power [kW]	12936	12900
average TLE outlet temperature [K]	775.6	775.2
average ethene yield [wt %]	27.9	27.88
average propene yield [wt %]	14.85	14.85
mixing-cup average *P/E*	0.5333	0.5338
convection section		
total heat exchanged [kW]	29935	29028
power feed preheat [kW]	19620	19593
power energy recovery [kW]	10316	9435
percentage feed preheat [%]	65.54	67.50
percentage energy recovery [%]	34.46	32.50
stack temperature [K]	120.1	119.3

various iterative loops indicated in Figure 2. There is no significant shift in heat flux to each individual reactor when comparing both cases as shown in Figure 5a. This results in a similar maximum TMT, coil outlet temperature, and propene-to-ethene, $(P/E)_i$, ratio as shown in Figure 5b, c, and d, respectively.

Due to the coating on the reactor tubes in the high emissivity case, the heat input via radiation is 1.69% higher in the high emissivity case compared to the low emissivity case. In absolute terms, 77.88% of the thermal power is delivered to the reactor coils via radiation in the low emissivity case, but this increases to 79.33% in the high emissivity case. Due to the more efficient heat transfer via radiation, less energy is transferred via convection from the flue gas to the reactor coils so the temperature of the flue gas decreases; in particular, the bridge wall temperature decreases from 1370 K in the low emissivity case to 1356 K in the high emissivity case. Not only the temperature of the flue gas decreases but also the flow rate: 1.73% less fuel is required to maintain the cracking severity in the high emissivity case compared to the low emissivity case. As the air flow rate decreases accordingly to maintain the same air-to-fuel ratio, this implies a difference between 22.29 kg/s flue gas in the low emissivity case and 21.91 kg/s flue gas in the high emissivity case. Figure 5e and f show the net radiative heat input per coil and the radiative contribution to the heat flux per coil. Depending on the position of the coil relative to the burner, the total heat input (Figure 5a) and net radiative heat input (Figure 5e) can fluctuate about 3.5% around the mean value, leading to a different performance, a different coking rate, and hence a difference between individual coils in the on-stream time before one of the two decoking criteria is reached. Ultimately, the run length of the furnace is determined by the first coil that reaches its maximum on-stream time. The potential extra on-stream time of the other coils cannot be valorized since the decoking procedure has to be started for the entire furnace. Therefore, large differences in coking rate between coils in the same furnace decreases the overall furnace capacity.

The 3D simulation of the radiant section also allows visualization of important process variables in the furnace. Figure 6 shows on the one hand the reactors colored by tube metal temperatures and on the other hand the isosurface of 1.5 wt % O_2 colored by process gas velocity magnitude. The isosurface of the oxygen content in the flue gas provides a visual representation of the flame shape. The velocity magnitude colors show that the flue gas close to the wall flows the fastest and that it slows down toward the middle of the furnace. The staged burners in the USC furnace are designed to have the combustion region as close as possible to the furnace wall to minimize the risk of flame rollover and hence impingement of the flame on the reactor coils, which can cause considerable harm to the reactors. Their adequacy is confirmed as the major combustion regions are indeed located close to the furnace wall.

4.2. Transfer Line Exchanger. As seen from the reactor simulations, the mixing-cup averaged coil outlet temperature of the low emissivity case, 1146.1 K, is only slightly higher than that of the high emissivity case, 1145.3 K. The hot reactor effluent is cooled down in the transfer line exchanger to 775.6 and 775.2 K respectively, see Table 4. The small differences in TLE inlet temperature and outlet temperature between the high and the low emissivity case explain the small differences in total exchanged duty (12.94 MW in the low emissivity case versus 12.90 MW in the high emissivity case), resulting in a decrease in steam production of 0.014 kg/s, which is negligible since it is smaller than the convergence tolerance for the iterative optimization routines.

4.3. Convection Section. Table 4 also gives the lumped values for the convection section. As the flue gas flow rate and bridge wall temperature are lower in the high emissivity case compared to the low emissivity case, the total power available for heat exchange with the process gases in the convection section is also lower. The total power in the low emissivity case is 29.96 MW versus 29.03 MW in the high emissivity case, a difference of 3.10%. However, as the hydrocarbon feed and the dilution steam are to be heated to the same temperature in both the low emissivity and high emissivity cases, the power for feed preheat is nearly identical, with a negligible difference that can be attributed to the convergence tolerance. This implies that the difference is almost entirely situated in the energy recovery, i.e., the preheating of the boiler feedwater and the superheating of the high pressure steam. Indeed, as seen in Table 3, the injection of additional boiler feedwater in the second high pressure steam superheater bank (HPSSH-II) to control the temperature of the superheated steam is omitted in the high emissivity case. Additionally, the size of the fins on the HPSSH-II bank is reduced from 0.0127 m in the low emissivity case to 0.0030 m in the high emissivity case to take up less heat in this bank. Figure 7 illustrates the temperatures of the flue gas

DOI: 10.1021/acs.iecr.8b04068
Ind. Eng. Chem. Res. XXXX, XXX, XXX−XXX

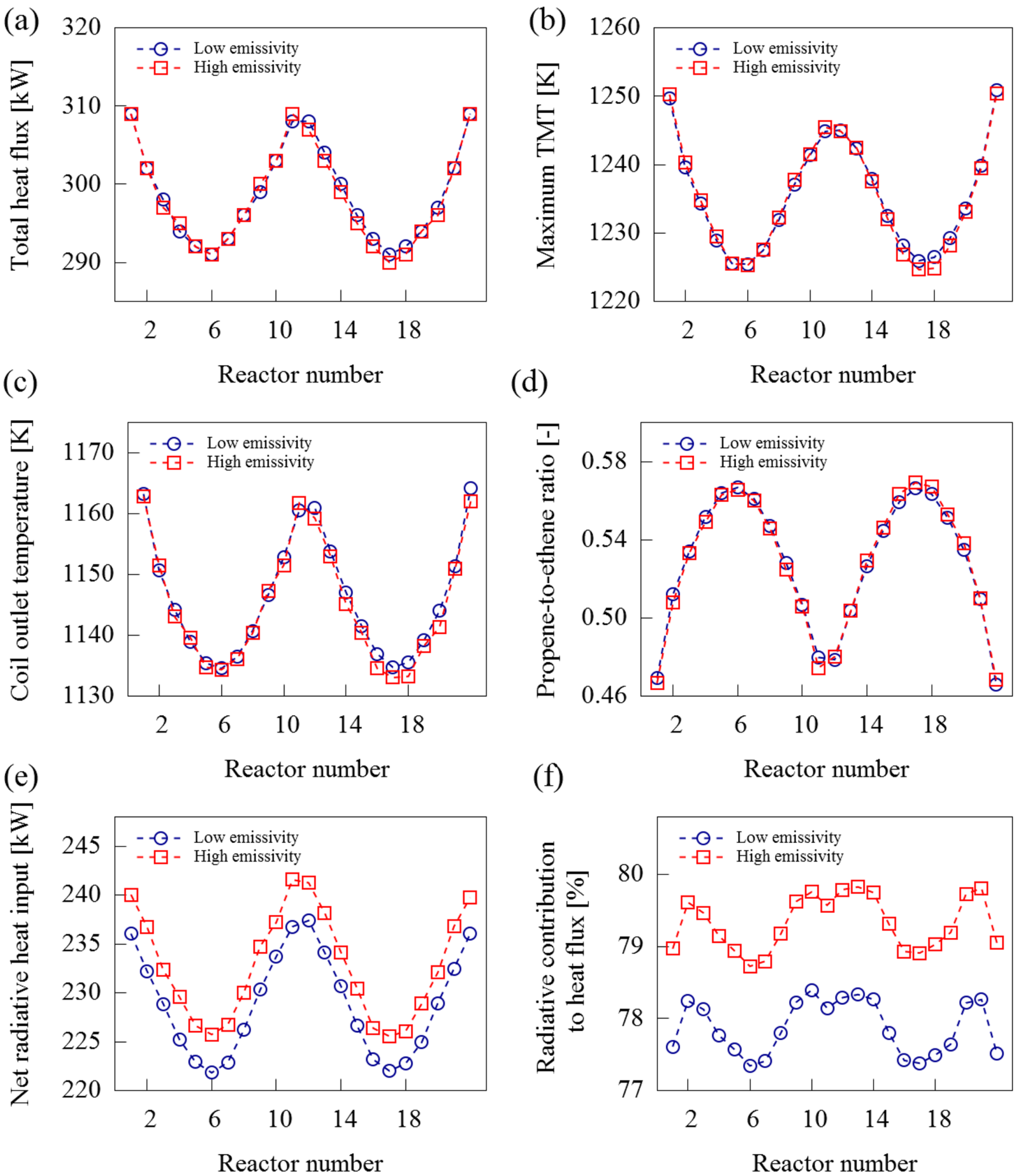

Figure 5. (a) Total heat flux, (b) maximum tube metal temperature, (c) coil outlet temperature, (d) propene-to-ethene ratio, (e) net radiative heat input, and (f) contribution from radiation to the total heat flux for every reactor coil.

and the process gases in the convection section for both the low emissivity case and the high emissivity case. The major difference is situated in the high pressure steam superheater banks 5 and 6. Especially in bank 6, in the low emissivity case due to the injection of additional boiler feedwater, the temperature of steam entering bank 6 decreases. As this injection is not done in the high emissivity case, the inlet temperature of bank 6 is higher. However, as the height of the fins in bank 6 is reduced, less heat is absorbed in this bank so the final temperature of the superheated steam is slightly lower in the high emissivity case compared to the low emissivity case. This difference in performance of bank 5 and bank 6 is necessary to ensure that the stack temperature is the same in the high emissivity case and the low emissivity case.

4.4. Overall Energy Balance. The overall energy balance of the simulated steam cracking process obtained by combining the results of the radiant section and reactors, the transfer line exchanger, and the convection section is shown in Table 5 and graphically represented in Figure 8.

The total fired duty is 1.73% lower in the high emissivity case compared to the low emissivity case since it was adapted to maintain the same cracking severity in both cases. Since the amount of heat absorbed by the reactors and the thermal losses from the radiant section to the environment are very similar in both cases, applying the high emissivity coating to the reactor outer wall increases the efficiency of the radiant section from 45.68% in the low emissivity case to 46.40% in the high emissivity case. The TLE recovers in both cases 50.0% of the energy absorbed by the reactors by cooling the process gas effluent to an average TLE outlet temperature of 775 K. When compared to the total fired duty, the TLE uses 22.84% in the low emissivity case and 23.18% in the high emissivity case to generate saturated high pressure steam, which is relatively low compared to the typical value for industry of around 29%.[36]

DOI: 10.1021/acs.iecr.8b04068
Ind. Eng. Chem. Res. XXXX, XXX, XXX−XXX

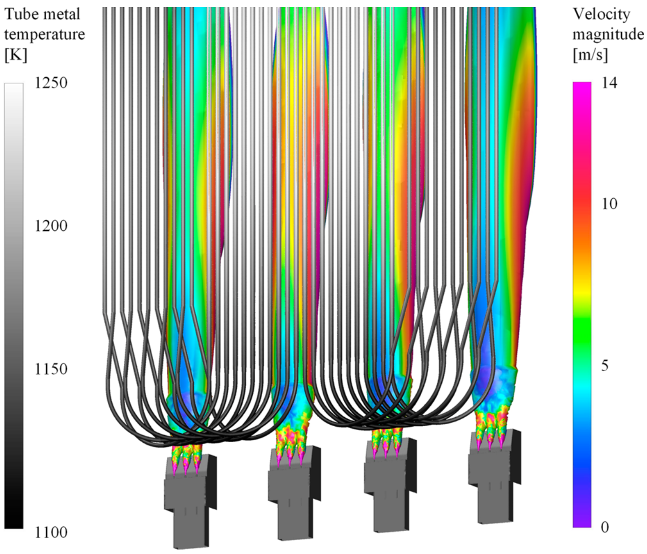

Figure 6. Reactors colored by outer wall temperature (left legend) and isosurface of 1.5 wt % O_2 colored by velocity magnitude (right legend); high emissivity case.

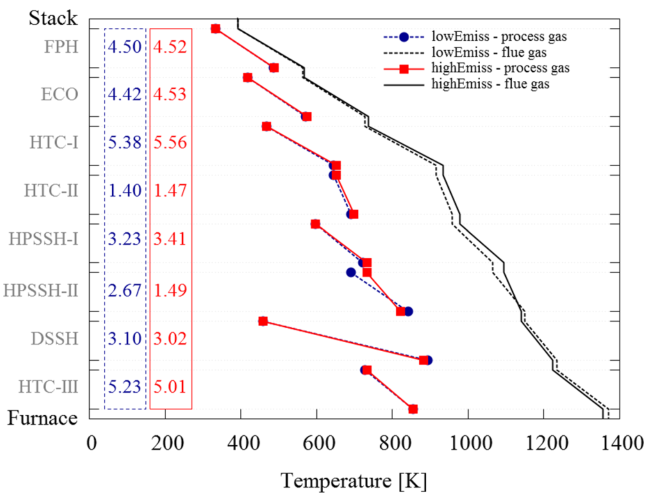

Figure 7. Temperature profiles in the convection section for process gas and flue gas in the low emissivity and high emissivity cases. Power [MW] per bank in the low emissivity case (blue dashed box) and the high emissivity case (red full box).

Table 5. Overall Energy Balance over the Entire Steam Cracking Unit

	low emissivity	high emissivity
total fired duty [kW]	56628	55652
total reactor duty [kW]	25868	25820
total preheating duty convection section [kW]	19620	19593
total energy recovery duty convection section [kW]	10316	9435
total losses from radiant section [kW]	566	566
total losses through stack [kW]	259	238
furnace efficiency [%]	45.68	46.40

Further lowering the TLE outlet temperature by adding additional heat transfer surface area could increase the energy recovery from the process gas effluent. The convection section recovers the remaining heat from the flue gas from the radiant section via feed preheating on one hand and energy recovery on the other hand. Feed preheating amounts to 34.65% of the total fired duty in the low emissivity case compared to 35.21% in the high emissivity case. The largest difference between the two cases is in the energy recovery part of the convection section: 18.22% of the total fired duty is used to generate high pressure steam in the low emissivity case versus 16.95% in the high emissivity case. Losses in both cases amount to 1.45% of the total fired duty, which is relatively low but acceptable for a modern furnace.

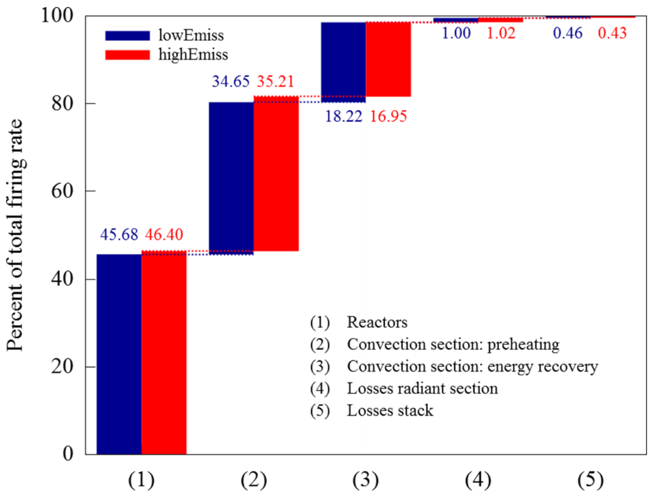

Figure 8. Overall energy balance over the entire steam cracking unit.

To answer the question whether applying a high emissivity coating to the reactor tubes in a steam cracking furnace is beneficial from an operational point of view, the totality of the plant is to be considered. Indeed, the mass and energy balances over the entire steam cracking unit indicate that for the same production rates, lower fuel flow rates are required, which lowers production costs and reduces harmful emissions. The efficiency of the radiant section is increased, but the overall efficiency of the complete steam cracking unit remains the same as indicated in Table 5. The heat losses to the environment and the amount of heat lost in the stack remain the same, so does the overall efficiency calculated to be 98.55% in this case. Applying the high emissivity coating shifts some of the heat from the convection section to the radiant section so less power is available in the convection section for steam generation. As this steam is used in other parts of the plant, for example to drive the steam turbine of the cracked gas compressor and the compressors of the ethene and propene refrigeration cycles, the duty spent for generating this steam cannot be considered as losses. When the high pressure steam production from the convection section decreases, it has to be produced in dedicated steam boilers with an average efficiency of around 85% since the total steam demand in the plant does not change. High emissivity coatings are hence relevant for an industrial steam cracking unit as a way of debottlenecking the olefin production process: the improved heat transfer to the coils increases the olefin production at the same firing rate. This is under the assumption that there are no other bottlenecks in the furnace, such as the maximum bridge wall temperature.

Increasing the furnace efficiency is also advantageous from an environmental point of view. Emissions of greenhouse gases, in particular NO_x components, correlate to the

DOI: 10.1021/acs.iecr.8b04068
Ind. Eng. Chem. Res. XXXX, XXX, XXX−XXX

prevailing temperatures in the furnace.[37,38] Indeed, an improved furnace efficiency implies lower maximum flue gas temperatures and hence also lower thermal NO_x formation. Contrary to fuel NO_x or prompt NO_x, thermal NO_x formed via the Zeldovich mechanism increases rapidly with increasing temperature.[39] Therefore, the decrease in average flue gas temperature in the radiant section of 12 K—from 1450 K in the low emissivity case to 1438 K in the high emissivity case—is expected to have a beneficial effect on the NO_x emissions.

Even though applying high emissivity coatings offers a way to improve the thermal efficiency of an industrial steam cracking unit,[40] their use on reactor coils in industrial steam cracker units is far from widespread for several reasons. *First*, little information is available on the lifetime of the high emissivity coating. Possible hot spot formation due to spallation has not been studied yet. *Second*, soot deposition on the coating has to be prevented because when it covers the surface, the beneficial effect of the coating is negated. *Third*, generally the spectral emissivity of the uncoated surface of steam cracking reactors is already high, reducing the potential for a high emissivity coating to improve the performance.[41,42] The potential is significantly higher for the refractory walls as the emissivity of the commonly used materials such as silica bricks or fiber insulation is inherently low. Coating these surfaces would increase the furnace efficiency considerably. *Fourth*, the effect of the selected coating on the material itself is yet to be determined. Diffusion from the coating material into the surface on which it is applied, in the process changing the material properties, has to be avoided or the consequences at least have to be studied. *Fifth*, an important concern is whether the decrease in operating cost originating from a lower fuel consumption outweighs the investment cost.

5. CONCLUSIONS

High emissivity coatings have the potential to increase the efficiency of high temperature industrial applications by enhancing the heat transfer via radiation. Applications of such coatings are already found in several industries, but others are hesitant to implement it as the longevity of the coating or its impact on the substrate material is yet to be determined. According to the literature, applying high emissivity coatings to the reactor tubes and/or the refractory walls of an industrial steam cracker can increase the furnace efficiency by up to 5% absolute, but the influence of the higher furnace efficiency on the convection section and the transfer line were not determined. Coupled 3D radiant section−1D reactor simulations of the ultra selective conversion U-coil furnace combined with 1D simulations of the convection section and the transfer line exchanger allowed assessment of the effects of applying a high emissivity coating to the reactor coils on the energy balance of the entire unit. The radiant box efficiency increased by 0.7% from 45.7 for uncoated reactors to 46.4% for coated reactors while the firing rate was decreased by 1.73% to maintain the same cracking severity. As the operating conditions for the process side were identical in both cases, the differences in the results for the reactor simulations and the transfer line exchanger were negligible. However, the flue gas flow rate and bridge wall temperature differed due to the changed firing rate. To ensure preheating of the process gas stream to the desired coil inlet temperature, less heat was to be used in the convection section for high pressure steam superheating in the high emissivity case. By eliminating secondary boiler feedwater injection and decreasing the fin size on the second high pressure steam superheater bank, the available duty in the convection section of the high emissivity case was correctly balanced between feed preheating and steam superheating. A total of 18.22% of the fired duty was used to generate high pressure steam in the base case versus 16.95% in the high emissivity case. Overall, the benefits in terms of energy of applying a high emissivity coating to the reactor outer walls are limited, in particular because the emissivity of the uncoated reactor material is already high. A more significant impact is expected when the high emissivity coating is also applied to the refractory walls. Even though the effect on the energy balance is low, a beneficial side effect of the lower average flue gas temperature in the radiant section is reduced formation of thermal NO_x and hence lower greenhouse gas emissions.

■ ASSOCIATED CONTENT

Ⓢ Supporting Information

The Supporting Information is available free of charge on the ACS Publications website at DOI: 10.1021/acs.iecr.8b04068.

> (Table S1) Geometry details and operating conditions of the ultra selective conversion furnace; (Table S2) geometry details of the adiabatic section and transfer line exchanger, operating conditions of the transfer line exchanger; (Table S3) geometry details of the convection section (DOCX)

■ AUTHOR INFORMATION

Corresponding Author

*E-mail: Kevin.VanGeem@UGent.be.

ORCID

Pieter A. Reyniers: 0000-0001-6794-6106

Guy B. Marin: 0000-0002-6733-1213

Kevin M. Van Geem: 0000-0003-4191-4960

Notes

The authors declare no competing financial interest.

■ ACKNOWLEDGMENTS

P.R. acknowledges financial support from a doctoral fellowship from the Research Foundation—Flanders (FWO). The authors also acknowledge the financial support from the Long Term Structural Methusalem Funding by the Flemish Government—grant number BOF09/01M00409. The work performed in the IMPROOF project contributed to this publication. The IMPROOF project has received funding from the European Union Horizon H2020 Programme (H2020-SPIRE-04-2016) under grant agreement no. 723706. The authors also would like to acknowledge the PRETREF project funded by Ghent University (Belgium) through GOA project BOF16/GOA/004. The computational work was carried out using the STEVIN Supercomputer Infrastructure at Ghent University, funded by Ghent University, the Flemish Supercomputer Center (VSC), the Research Foundation—Flanders (FWO) and the Flemish Government—department EWI. The authors would like to thank Pieter Verhees for his support with the simulations of the convection section.

■ NOTATION

Roman Symbols

c = light velocity in vacuum, m/s

$c_{p,j}$ = molar heat capacity of species j, J/mol/K

d = internal diameter, m
E = specific total energy, J/kg
f = Fanning friction factor, -
F_j = molar flow rate of species j, mol/s
h = Planck constant, J/s
h_j = specific enthalpy of species j, J/kg
h_f = heat transfer coefficient, W/m^2/K
I = radiation intensity, W/m^2
I_b = blackbody radiation intensity, W/m^2
$\overline{J_j}$ = diffusional flux of species j, kg/m^2/s
k_B = Boltzmann constant, J/K
k_{eff} = effective thermal conductivity, W/m/K
n = refractive index, -
$\vec{n}$ = normal pointing out of the domain, -
N_R = number of reactions, -
n_{spec} = number of species, -
p = total pressure, Pa
P/E = propene-to-ethene mass ratio, -
q = specific heat flux, W/m^2
$\vec{r}$ = position vector, -
r_i = molar rate of reaction i, mol/m^3/s
r_b = radius of a bend, m
R_j = net rate of formation of species j, mol/m^3/s
$\vec{s}$ = unit direction vector, -
S_h = energy source term, J/m^3/s
S_M = momentum source term, kg/m^2/s^2
T = temperature, K
u = velocity magnitude, m/s
$\overline{u}$ = velocity vector
V_m = molar volume m^3/mol
Y_j = mass fraction of species j, -
z = axial position, m

Greek symbols

ΔH_i, = molar enthalpy of reaction i, kJ/mol
ε_w = emissivity of the wall, -
ζ = Nekrasov factor for bends, -
κ = absorption coefficient, 1/m
λ = wavelength, μm
ρ = density, kg/m3
σ = Stefan−Boltzmann constant, W/m^2/K^4
$\overline{\overline{\tau}}$ = stress tensor, Pa

Subscripts and Superscripts

f = fluid
in = incident
out = outward
w = wall
rad = radiation

Abbreviations

BFW = boiler feedwater
BWT = bridge wall temperature
CFD = computational fluid dynamics
DO = discrete ordinates
DSSH = dilution steam superheater
ECO = economizer convection bank
EDR = exchanger design and rating
EWBM = exponential wide band model
FPH = feed preheater
HP = high pressure
HPPSH = high pressure steam superheater
HTC = high temperature convection
RANS = Reynolds-averaged Navier−Stokes
RNG = renormalization group
TLE = transfer line exchanger
TMT = tube metal temperature
USC = ultra selective conversion
XOT = crossover temperature

REFERENCES

(1) Yao, Z.; Xia, Q.; Ju, P.; Wang, J.; Su, P.; Li, D.; Jiang, Z. Investigation of absorptance and emissivity of thermal control coatings on Mg−Li alloys and OES analysis during PEO process. *Sci. Rep.* **2016**, *6*, 29563.
(2) Okuhara, Y.; Yokoe, D.; Kato, T.; Suda, S.; Takata, M.; Noritake, K.; Sato, A. Solar-selective absorbers based on semiconducting β-FeSi2 for efficient photothermal conversion at high temperature. *Sol. Energy Mater. Sol. Cells* **2017**, *161*, 240−246.
(3) Shao, G.; Wu, X.; Kong, Y.; Shen, X.; Cui, S.; Guan, X.; Jiao, C.; Jiao, J. Microstructure, radiative property and thermal shock behavior of TaSi2−SiO2-borosilicate glass coating for fibrous ZrO2 ceramic insulation. *J. Alloys Compd.* **2016**, *663*, 360−370.
(4) Raman, A. P.; Anoma, M. A.; Zhu, L.; Rephaeli, E.; Fan, S. Passive radiative cooling below ambient air temperature under direct sunlight. *Nature* **2014**, *515*, 540.
(5) Howell, J. R.; Menguc, M. P.; Siegel, R. *Thermal Radiation Heat Transfer*, 6th ed.; CRC Press, 2015.
(6) Tucker, R.; Ward, J. Identifying and quantifying energy savings on fired plant using low cost modelling techniques. *Appl. Energy* **2012**, *89* (1), 127−132.
(7) Benko, I. High infrared emissivity coating for energy conservation and protection of inner surfaces in furnaces. *International Journal of Global Energy Issues* **2002**, *17* (1−2), 60−67.
(8) Brown, D. J.; Smith, P. J.; Adams, B. R. Cracking furnace fireside modeling advances. In *6th Ethylene Producers' Conference*, Atlanta, GA, USA, 1994.
(9) Brown, D. J.; Cremer, M. A.; Smith, P. J.; Waibel, R. T. Fireside modeling in cracking furnaces. In *9th Ethylene Producers' Conference*, Houston, TX, USA, 1997.
(10) Tang, Q.; Denison, M.; Adams, B.; Brown, D. Towards comprehensive computational fluid dynamics modeling of pyrolysis furnaces with next generation low-NOx burners using finite-rate chemistry. *Proc. Combust. Inst.* **2009**, *32* (2), 2649−2657.
(11) Oprins, A. J. M.; Heynderickx, G. J.; Marin, G. B. Three-Dimensional Asymmetric Flow and Temperature Fields in Cracking Furnaces. *Ind. Eng. Chem. Res.* **2001**, *40* (23), 5087−5094.
(12) Habibi, A.; Merci, B.; Heynderickx, G. J. Impact of radiation models in CFD simulations of steam cracking furnaces. *Comput. Chem. Eng.* **2007**, *31* (11), 1389−1406.
(13) Stefanidis, G. D.; Merci, B.; Heynderickx, G. J.; Marin, G. B. Gray/nongray gas radiation modeling in steam cracker CFD calculations. *AIChE J.* **2007**, *53* (7), 1658−1669.
(14) Modest, M. F. The treatment of nongray properties in radiative heat transfer: from past to present. *J. Heat Transfer* **2013**, *135* (6), 061801.
(15) Edwards, D. K.; Balakrishnan, A. Thermal radiation by combustion gases. *Int. J. Heat Mass Transfer* **1973**, *16* (1), 25−40.
(16) Zhang, Y.; Qian, F.; Schietekat, C. M.; Van Geem, K. M.; Marin, G. B.; Zhang, Y. Impact of flue gas radiative properties and burner geometry in furnace simulations. *AIChE J.* **2015**, *61* (3), 936−954.
(17) Zhang, Y.; Reyniers, P. A.; Schietekat, C. M.; Van Geem, K. M.; Marin, G. B.; Du, W.; Qian, F. Computational fluid dynamics-based steam cracking furnace optimization using feedstock flow distribution. *AIChE J.* **2017**, *63* (7), 3199−3213.
(18) Hu, G.; Schietekat, C. M.; Zhang, Y.; Qian, F.; Heynderickx, G.; Van Geem, K. M.; Marin, G. B. Impact of Radiation Models in Coupled Simulations of Steam Cracking Furnaces and Reactors. *Ind. Eng. Chem. Res.* **2015**, *54* (9), 2453−2465.
(19) Zhang, Y.; Reyniers, P. A.; Du, W.; Qian, F.; Van Geem, K. M.; Marin, G. B. Incident Radiative Heat Flux Based Method for the

DOI: 10.1021/acs.iecr.8b04068
Ind. Eng. Chem. Res. XXXX, XXX, XXX−XXX

Coupled Run Length Simulation of Steam Cracking Furnaces. *Ind. Eng. Chem. Res.* **2017**, *56* (14), 4156−4172.
(20) Heynderickx, G. J.; Nozawa, M. High-emissivity coatings on reactor tubes and furnace walls in steam cracking furnaces. *Chem. Eng. Sci.* **2004**, *59* (22−23), 5657−5662.
(21) Heynderickx, G. J.; Nozawa, M. Banded gas and nongray surface radiation models for high-emissivity coatings. *AIChE J.* **2005**, *51* (10), 2721−2736.
(22) Stefanidis, G. D.; Van Geem, K. M.; Heynderickx, G. J.; Marin, G. B. Evaluation of high-emissivity coatings in steam cracking furnaces using a non-grey gas radiation model. *Chem. Eng. J.* **2008**, *137* (2), 411−421.
(23) Verhees, P.; Amghizar, I.; Goemare, J.; Akhras, A. R.; Marin, G. B.; Van Geem, K. M.; Heynderickx, G. J. 1D Model for Coupled Simulation of Steam Cracker Convection Section with Improved Evaporation Model. *Chem. Ing. Tech.* **2016**, *88* (11), 1650−1664.
(24) Vervust, A.; Amghizar, I.; Muñoz Gandarillas, A. E.; Van Geem, K. M.; Marin, G. B., Full Furnace Simulation and Optimization with COILSIM1D. In *AIChE Spring Meeting, The 28th Ethylene Producers' Conference*, Houston, TX, USA, 2016.
(25) Boussinesq, J. *Essai Sur la Théorie des Eaux Courantes*; Imprimerie Nationale, 1877.
(26) Launder, B. E.; Spalding, D. B. The numerical computation of turbulent flows. *Computer Methods in Applied Mechanics and Engineering* **1974**, *3* (2), 269−289.
(27) Westbrook, C. K.; Dryer, F. L. Simplified Reaction Mechanisms for the Oxidation of Hydrocarbon Fuels in Flames. *Combust. Sci. Technol.* **1981**, *27* (1−2), 31−43.
(28) Stefanidis, G. D.; Merci, B.; Heynderickx, G. J.; Marin, G. B. CFD simulations of steam cracking furnaces using detailed combustion mechanisms. *Comput. Chem. Eng.* **2006**, *30* (4), 635−649.
(29) Magnussen, B. F.; Hjertager, B. H. On mathematical modeling of turbulent combustion with special emphasis on soot formation and combustion. *Symp. (Int.) Combust., [Proc.]* **1977**, *16* (1), 719−729.
(30) Yeoh, G. H.; Yuen, K. K. *Computational Fluid Dynamics in Fire Engineering: Theory, Modelling and Practice*; Elsevier Science, 2009.
(31) Baukal, C. E.; Gershtein, V.; Li, X. J. *Computational Fluid Dynamics in Industrial Combustion*; Taylor & Francis, 2000.
(32) Khan, W. A.; Culham, J. R.; Yovanovich, M. M. Convection heat transfer from tube banks in crossflow: Analytical approach. *Int. J. Heat Mass Transfer* **2006**, *49* (25), 4831−4838.
(33) Shah, R.; Mueller, A. Heat exchanger basic thermal design methods. *Handbook of Heat Transfer Applications*; McGraw-Hill: New York, 1985; Vol 2.
(34) Verhees, P.; Akhras, A. R.; Van Geem, K. M.; Heynderickx, G. J. Fouling in a Steam Cracker Convection Section Part 1: A Hybrid Computational Fluid Dynamics One-Dimensional Model to Obtain Accurate Tube Wall Temperature Profiles. *Heat Transfer Eng.* **2018**, 1−35.
(35) Van Geem, K. M.; Reyniers, M.-F.; Marin, G. B. Two Severity Indices for Scale-Up of Steam Cracking Coils. *Ind. Eng. Chem. Res.* **2005**, *44* (10), 3402−3411.
(36) Zimmermann, H.; Walzl, R. Ethylene. In *Ullmann's Encyclopedia of Industrial Chemistry*; Wiley-VCH Verlag GmbH & Co. KGaA, 2000.
(37) Hassan, G.; Pourkashanian, M.; Ingham, D.; Ma, L.; Newman, P.; Odedra, A. Predictions of CO and NOx emissions from steam cracking furnaces using GRI2.11 detailed reaction mechanism − A CFD investigation. *Comput. Chem. Eng.* **2013**, *58*, 68−83.
(38) Isaacs, R. K.; Marty, S. A.; Barnes, J. E. In *Flameless Combustion Technology for Reduced NOx Emissions in Ethylene Furnaces*; AIChE Spring National Meeting, New Orleans, LA, USA, 2014.
(39) Baukal, C. E. *The John Zink Hamworthy Combustion Handbook*, Second ed.; Taylor & Francis, 2012; Vol. *1* - Fundamentals.
(40) Švantner, M.; Honnerová, P.; Veselý, Z. The influence of furnace wall emissivity on steel charge heating. *Infrared Phys. Technol.* **2016**, *74*, 63−71.
(41) Cao, G.; Weber, S. J.; Martin, S. O.; Anderson, M. H.; Sridharan, K.; Allen, T. R. Spectral emissivity measurements of candidate materials for very high temperature reactors. *Nucl. Eng. Des.* **2012**, *251*, 78−83.
(42) Van Geem, K. M.; Battin-Leclerc, F.; Bellos, G.; Heynderickx, G. J.; Buysschaert, W.; Cuenot, B.; Djokic, M. R.; Faravelli, T.; Theis, G.; Jakobi, D.; Lenain, P.; Muñoz Gandarillas, A. E.; Olver, J.; Dedeyne, J.; Vangaever, S.; Honnerová, P.; Veselý, Z. IMPROOF: Integrated Model Guided Process Optimization of Steam Cracking Furnaces. In *29th Ethylene Producers' Conference*, San Antonio, TX, USA, 2017.

DOI: 10.1021/acs.iecr.8b04068
Ind. Eng. Chem. Res. XXXX, XXX, XXX−XXX